energies

Article

Application of the Source Term Method and Fan-Shaped Hole for Cooling Performance Improvement in a High-Pressure Turbine

Sangook Jun *, Dong-Ho Rhee, Young Seok Kang, Heeyoon Chung and Jae-Hwan Kim

Aeropropulsion Research Division, Korea Aerospace Research Institute, Daejeon 34133, Korea
* Correspondence: sangookjun@kari.re.kr

Abstract: This study presents the arrangement design of the cooling hole and the application of a fan-shaped hole to improve the cooling performance of the high-pressure turbine. To this end, the first stage nozzle vane of the energy efficient engine (E3) was selected as the base model, and for efficient design, the source term method, called the injection region, was applied for producing the effect of the cooling flow when the RANS analysis was performed. At this time, because the cooling flow rate also changed when the location of the cooling hole changed, a neural network model was constructed to predict the cooling flow rate for the location of the cooling hole. Design optimization was performed to improve the film cooling effectiveness and the temperature uniformity on the vane surface using the streamwise location of the cooling hole as a design variable, and then the cooling performance was investigated by applying several fan-shaped holes instead of cylinder holes on the pressure side. As a result, the final design was obtained, which improved the film cooling effectiveness by 4.1%p and temperature uniformity by 0.7% compared with the base model.

Keywords: cooling design; fan-shaped film cooling hole; cooling hole arrangement design; source term method; approximate model; turbine nozzle

Citation: Jun, S.; Rhee, D.-H.; Kang, Y.S.; Chung, H.; Kim, J.-H. Application of the Source Term Method and Fan-Shaped Hole for Cooling Performance Improvement in a High-Pressure Turbine. *Energies* **2022**, *15*, 6943. https://doi.org/10.3390/en15196943

Academic Editor: Jiang Lei

Received: 1 September 2022
Accepted: 19 September 2022
Published: 22 September 2022

1. Introduction

Film cooling is a method to prevent the blade from making direct contact with high-temperature gas by flowing a cooling fluid on the blade surface to make a thin film. This helps to improve the efficiency of the turbine engine by making the turbine inlet temperature higher. In film cooling flow, the cooling fluid in the inner flow path of the blade is discharged to the surface of the blade through the cooling hole, and the cooling performance is different depending on the shape and location of the hole [1].

In this regard, research on the shape design of the cooling holes has been conducted in the past decades, and, recently, the interaction between the cooling holes and the installation location has also been considered [2–5]. Johnson et al. [6] optimized the shape and pattern of the cooling hole on the pressure side of the turbine nozzle vane, and Al-Zurfi et al. [7] studied how to reduce the vortex through LES analysis by placing three types of cooling holes in the 1-1/2 turbine stage. Liu et al. [8] installed six types of film cooling hole arrays at the endwall near the leading edge, and the cooling fluid coverage of these arrays was investigated according to the blowing ratio and turbulence intensity. Lee et al. [9] performed cooling hole arrangement design using robust design optimization so that the average temperature of the vane surface was uniform in consideration of the manufacturing uncertainty for the cooling hole. They designed the cooling hole array for the high-pressure turbine with the cooling system, and applied it to the surrogated model constructed from the conjugated heat transfer analysis, which has a high computing cost. In this way, research on the cooling hole design using numerical analysis for turbines requires a lot of computing resources and still has weaknesses, which make it difficult to increase the number of design variables because of the computing load. Therefore, a more efficient design method is needed.

The source term method can compensate for these defects that result from the numerical analysis of the film cooling flow. This method simulates the cooling flow discharged from the cooling hole exit without modeling the real cooling hole geometry, and many works considering this model have been conducted [10–12]. Research on the design optimization of turbine cooling holes using this source term method is rarely reported. Yang et al. [13] conducted multi-objective design optimization of the cooling hole located at the tip of the turbine blade. They performed topology optimization with objective functions to minimize energy loss and maximize the heat transfer rate, and found the layout of cooling holes that were uniformly arranged in an axial direction to have an improved performance compared with the baseline. Here, they selected the cooling flow rate as a design variable. However, if the cooling flow rate is not used as a design variable, it is difficult to specify its value because the internal cooling flow path is not considered in this method. Therefore, there is a need to find a way to predict the cooling flow rate with respect to the cooling hole location.

In this study, the first stage nozzle vane of the well-known energy efficient engine (E3) high-pressure turbine [14,15] was used as the base model, and the cooling design process was applied. The effect of the cooling performance improvement through the cooling hole arrangement design from a previous study [16] and a fan-shaped hole application was investigated, and the final model was derived from this design process. To this end, the streamwise location of the cooling holes was selected as the design variable in order to improve the film cooling effectiveness and temperature uniformity on the vane surface. In addition, for efficient design, the cooling performance was evaluated using the source term method called the injection region [17], which can simulate the effect of the cooling flow. A surrogated model was constructed to estimate the cooling flow rate for the cooling hole location. Lastly, by applying several fan-shaped holes to the design drawn from this cooling hole arrangement, the final design was obtained with a more improved cooling performance. Through these results, by comparing the base model, the cooling hole arrangement design, and the final design applying the fan-shaped hole, the effect of the cooling hole arrangement design and the fan-shaped hole application on the cooling performance was investigated.

2. Process of Cooling Design

The cooling design process carried out in this study is shown in Figure 1. Firstly, the base model was selected, the design problem was defined, and the cooling flow rate model was constructed to use the source term method. Then, after the approximate model was made for the efficient design, the cooling hole arrangement design was conducted. For the results obtained through this process, the full model including the cooling system, such as the internal cooling flow path and cooling holes, was made, and it was validated via Reynolds-Averaged Navier–Stokes (RANS) analysis. Additionally, the cooling performance was investigated by applying a cooling hole of the fan-shaped type. A series of processes for this turbine nozzle cooling design is described in more detail in the following chapter.

2.1. Base Model

The base model that is the target of the cooling design, as shown in Figure 2, is the first stage nozzle vane of E3 high-pressure turbine. It was modeled based on the airfoil and meridional plane information presented in NASA reports [14,15], and the cooling system was also referred to in the same references. However, because the information in them was not sufficient, the modeling for the base model was supplemented with other turbine shapes and a one-dimensional analysis. There are two cavities inside the vane, and an impingement plate is configured therein. About five to six compartments and inner/outer impingement plates are also installed on the endwall where the cooling fluid enters. The cooling fluid is supplied to the forward cavity through the inner band of the hub, and to the afterward cavity through the outer band of the shroud. In Figure 3, the cooling hole in the vane is composed of a total of 13 rows. The two cooling hole rows of the suction side have diffusion type, holes of the leading edge and the pressure side have a cylinder type, and the trailing edge has a slot type. For convenience, the rows of the cooling hole are marked with Row1 to 13 in a counterclockwise direction from the suction side to the trailing edge.

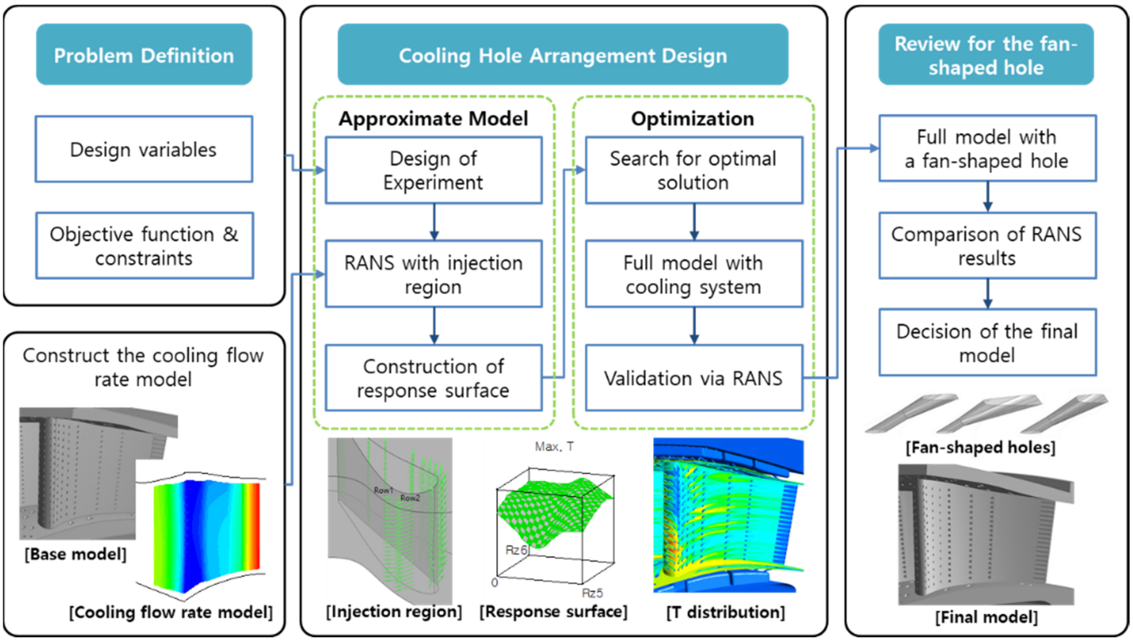

Figure 1. Cooling design flow considering a cooling hole arrangement and a fan-shaped hole (adapted with permission from [16]; copyright 2021 Korean Society for Fluid Machinery).

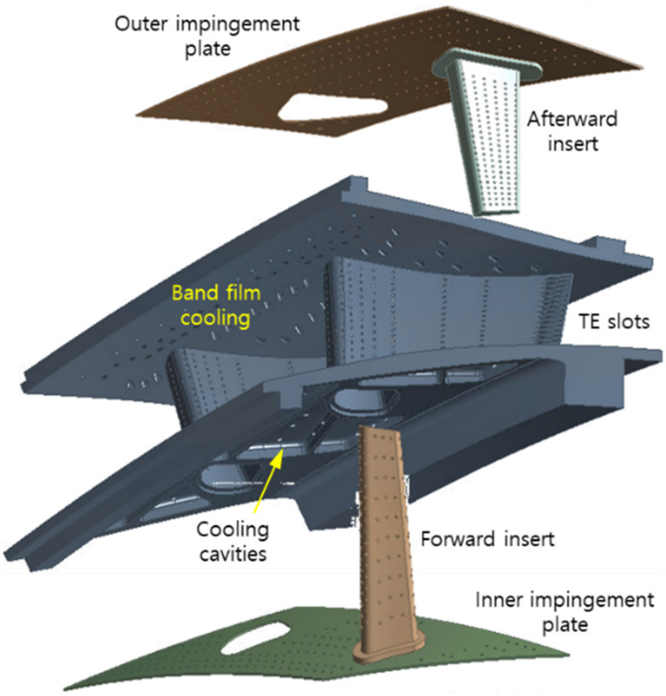

Figure 2. Base model—the first stage nozzle vane (reprinted with permission from [16]; copyright 2021 Korean Society for Fluid Machinery).

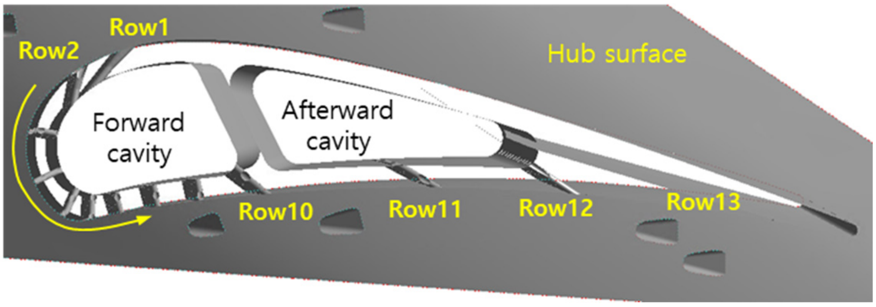

Figure 3. Cooling hole array (reprinted with permission from [16]; copyright 2021 Korean Society for Fluid Machinery).

2.2. Problem Definition and Cooling Flow Rate Model

As described in Figure 4, the relative streamwise location of the cooling hole exit was selected as a design variable to prevent the reverse of the order of the cooling hole rows, and the slot-type cooling hole at the trailing edge was excluded. The range of the design variables was intended to allow each cooling hole row to have a maximum space, and to connect Rows1~10 to the forward cavity and Rows11~13 to the afterward cavity. It is summarized in Table 1. The objective function was to improve the film cooling effectiveness (η) and the temperature uniformity (σ(T), the standard deviation of T) of the vane surface, and a weight of 1:1 ratio was given in order to obtain only one result. This means that the average temperature of the vane surface was lowered and the high temperature region was reduced to evenly distribute the temperature of the vane surface. The constraint was defined that the maximum temperature (T_{max}) at the vane was lower than that of the base model ($T_{max,\ Base\ model}$). The design problem defined in this way is presented in Equation (1), where T_∞ is main flow temperature, T_w is wall temperature, and T_c is the cooling flow temperature.

$$\begin{cases} \text{min.} \quad \eta + \sigma(T) \\ \text{subject to } T_{max} \leq T_{max,\ Base\ model} \end{cases} \quad \text{where, } \eta = \frac{T_\infty - T_w}{T_\infty - T_c} \tag{1}$$

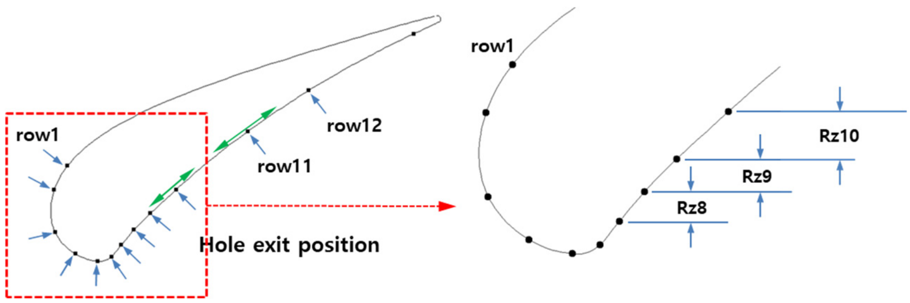

Figure 4. Definition of design variables (reprinted with permission from [16]; copyright 2021 Korean Society for Fluid Machinery).

The cooling design used the method of applying the source term to the location of the cooling hole to produce the film cooling flow. This method requires the location of the cooling hole exit and the cooling flow rate discharged from it. In this study, because the hole location was only used as a design variable, the cooling flow rate needed to be specified. However, this source term method does not actually model the internal flow path and cooling holes, so it is difficult to obtain the pressure distribution of the internal cooling flow path and the cooling flow rate. For this reason, a method to estimate the cooling flow rate for the cooling hole location is required. To this end, under the assumption that the pressure of the internal flow path and the vane surface would not change significantly even if the location of the cooling hole changed, the numerical analysis was performed for the base model with the cooling system, and then the neural network model to predict the cooling flow rate for the vane surface was constructed based on this result. This process to make the cooling flow rate model is presented in Figure 5. First, RANS was carried out on the base model with the cooling system, and the cooling flow rate discharged from each cooling hole was collected. From it, a dataset of the cooling flow rate for the coordinates of the cooling hole location was prepared. Because a neural network model was used as the cooling flow rate model in this study, this dataset was used to learn a neural network. After the learning stage finished, this neural net model provides the cooling flow rate for a given cooling hole location during the cooling hole arrangement design. It was confirmed that the cooling flow rate for the cooling hole location could be provided with a high reliability because this neural net model had a coefficient of determination (R^2) of 0.9994 and root mean square error (RMSE) of 1.09×10^{-4}.

Table 1. Range of design variables (reprinted with permission from [16]; copyright 2021 Korean Society for Fluid Machinery).

Design Variable	Lower Bound	Upper Bound
Rz1	0.08	0.2
Rz2	0.06	0.18
Rz3	0.03	0.1
Rz4	0.02	0.04
Rz5	−0.01	0.01
Rz6	0.02	0.04
Rz7	0.03	0.06
Rz8	0.04	0.08
Rz9	0.06	0.09
Rz10	0.08	0.1
Rz11	0.22	0.3
Rz12	0.15	0.2

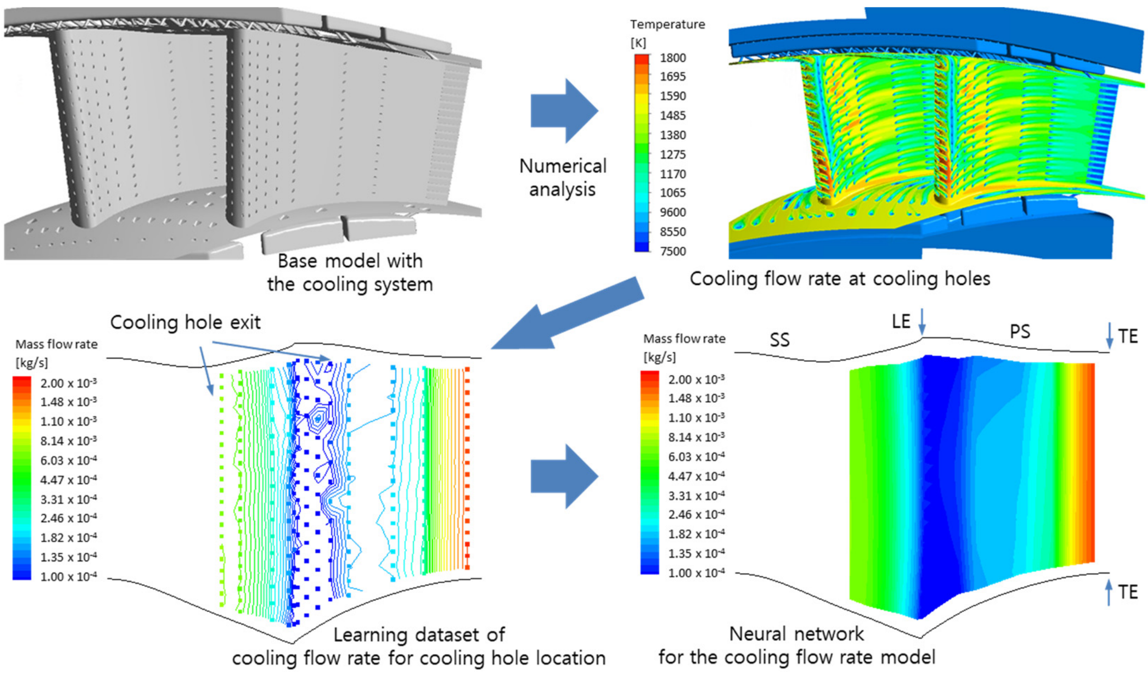

Figure 5. Process to construct the cooling flow rate model (unit: kg/s) (adapted with permission from [16]; copyright 2021 Korean Society for Fluid Machinery).

2.3. Aerodynamic Analysis

To evaluate the cooling performance, such as the film cooling effectiveness, maximum temperature, and temperature uniformity on the vane surface, ANSYS CFX v2020 [17], a commercial software, was used. RANS analysis for compressible flow was performed via this software, and the SST turbulent model was selected. The inlet and outlet boundary conditions of the main flow, as summarized in Table 2, were used, and the Re number in this case was 4.7×10^6. The computational domain was an uncooled vane shape, and 5.88 million structured grids were used. CFX provided the source term method called the injection region [17], where users can conveniently access the film cooling flow for turbine cooling. This method applies a source term where the cooling fluid is discharged at the cooling hole location with an ejection angle and hole diameter to simulate the film cooling flow, as shown in Figure 6. As the cooling hole does not needs to be modeled, the computational domain of the uncooled vane can be used immediately. Therefore, it is possible to significantly reduce the cost required for the numerical analysis. However, it must be taken into account that the cooling flow rate changed when the cooling hole location is moved on the vane surface. In this study, to predict this change in the cooling flow rate, the cooling flow rate model mentioned above was constructed and applied during the cooling hole arrangement design.

Table 2. Boundary conditions (adapted with permission from [16]; copyright 2021 Korean Society for Fluid Machinery).

Location	Condition	
Inlet	Total pressure Total temperature Turbulent intensity	2.526 MPa 1776 K 5%
Outlet	Averaged static pressure	1.52 MPa
Coolant inlet—Inner band	Total pressure Total temperature Turbulent intensity	2.61 MPa 883 K 5%
Coolant inlet—Outer band	Total pressure Total temperature Turbulent intensity	2.57 MPa 883 K 5%

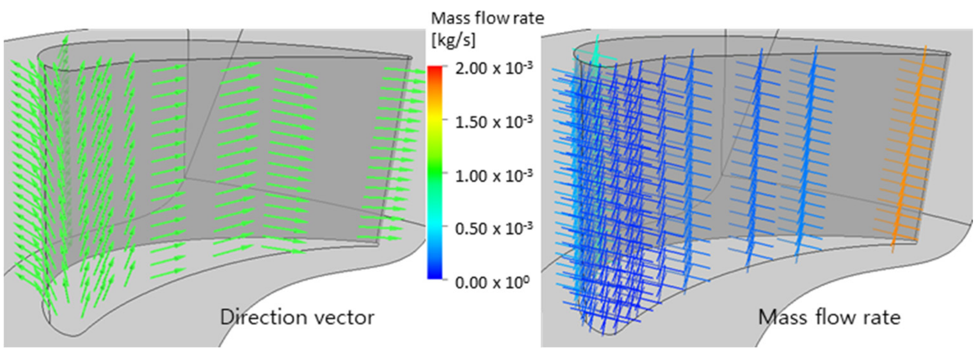

Figure 6. Injection region in the computational domain (eject direction and mass flow rate of the coolant). (reprinted with permission from [16]; copyright 2021 Korean Society for Fluid Machinery).

Generally, the flow ejected from the cooling hole is not uniform, but is deflected in one direction, which is not reflected in this source term method. For this reason, this method has a high possibility of predicting the temperature on the vane surface differently than the numerical analysis results of the model with the cooling system. However, as the change of the cooling hole location can be imitated by the movement of the source term, the trend in temperature variation is sufficiently predictable. In terms of computational cost, this method has a huge advantage over performing an analysis on a model with a cooling system. The model with the cooling system requires tens of millions of meshes, but the uncooled model used in the source term method only has millions of meshes. Table 3 shows the computational time required for the numerical analysis of the base model. The computation was performed on a High-Performance Computer (HPC) equipped with Intel® Xeon® Gold 6229R CPU 160core and 96GB RAM, and the mesh was generated using one core in the same system. The cost for RANS using the source term method is reduced to 1/10 for generating mesh and 1/90 for solving compared with RANS on the model with the cooling system. That is, while one full model calculation is performed, about 50 cases can be computed if the source term method is used. Because of this, it can be said that the source term method guarantees efficiency and a degree of freedom in design.

Table 3. Comparison of the computational cost for the base model.

	RANS on the Model with the Cooling System	RANS Using Source Term Method
Generate Mesh	1 h 50 min 48 s	11 min 3 s
Solve	15 h 36 min 46 s	10 min 28 s
Total	17 h 27 min 34 s	21 min 31 s

In the case of verifying the result of the cooling design using the source term method and investigating the cooling performance of a nozzle vane to which a fan-shaped hole was applied, a numerical analysis was performed for the turbine nozzle modeled with the cooling system, including the forward and after insert, inner and outer impingement plates, and cooling holes, as illustrated in Figure 2. The boundary conditions and solver applied were the same as those used in the cooling hole arrangement design, except the injection region, and the pressure and temperature conditions of the cooling fluid, were given to the inlets of the inner and outer bands, as summarized in Table 2, because there was no source term for the film cooling flow. Figure 7 presents this computational domain and mesh system. The number of grids for aerodynamic analysis was about 80 million and the mesh with y+ 5 was selected in this study through a grid test on y+.

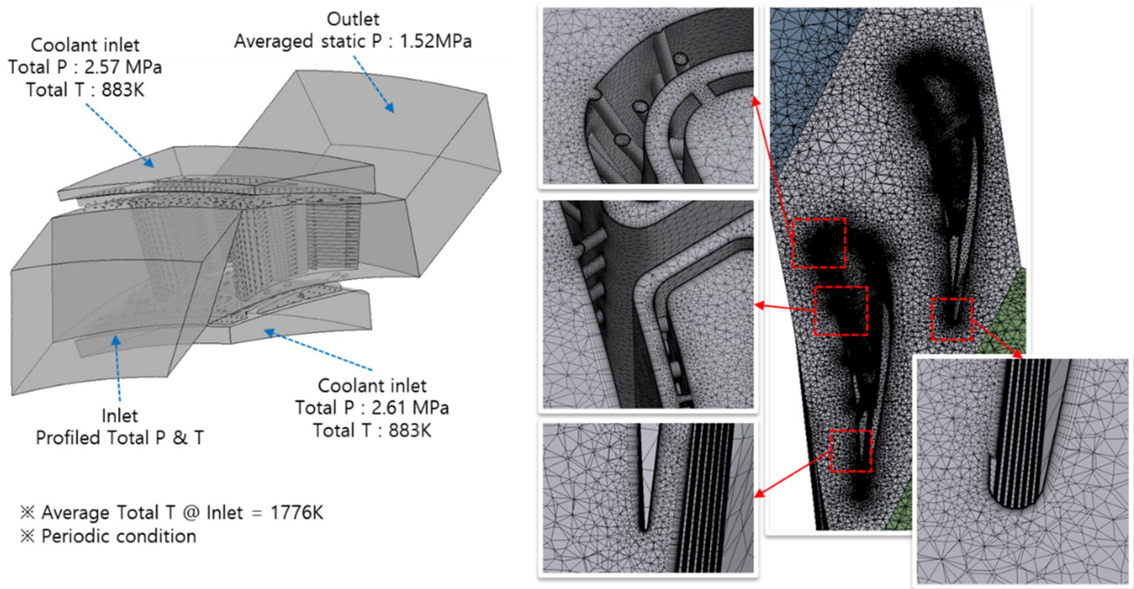

Figure 7. Computational domain including the cooling system and mesh system.

2.4. Construction of the Approximate Model

The design of the experiment method was used to construct an approximate model that could calculate the values of the objective function and constraints for the design space, as given in Table 1. The D-optimal method that minimizes the standard deviation of the distance between the experimental points was applied to make the experimental points evenly distributed in the design space, and a total of 137 experimental points were extracted because there were 12 design variables. Numerical analysis was performed for each of these experimental points, and the approximate model of second-order polynomial was constructed based on the temperature distribution of the vane surface obtained therefrom.

Using the approximate model made in this way, the sensitivity graphs of the film cooling effectiveness, maximum temperature, and temperature uniformity for the design variables are presented in Figure 8. Overall, it can be seen that all three indices are greatly affected by design variables Rz1, Rz5, and Rz6. Among them, Rz5 and 6 were located at the leading edge and near the stagnation points, and this region was directly faced with a high-temperature main flow. For this reason, it is conjectured that the maximum temperature was more sensitive than the other indices. Table 4 summarizes the reliability indices of the approximate model. As the coefficient of determination was 0.9 or higher, it is reasonable to perform the cooling hole arrangement design using these response surface models.

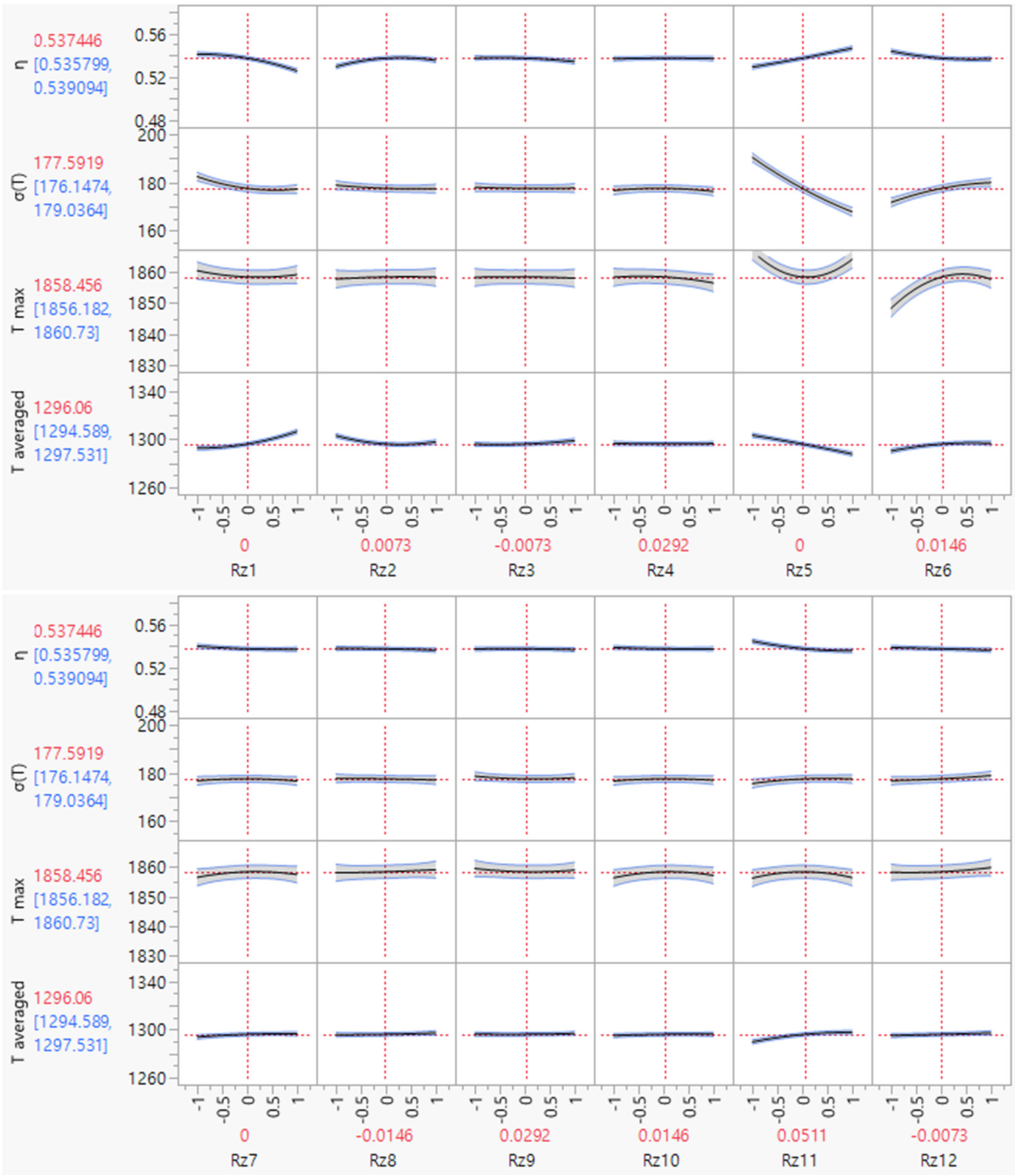

Figure 8. Sensitivity chart for the cooling performance (adapted with permission from [16]; copyright 2021 Korean Society for Fluid Machinery).

Table 4. Reliability index for approximate models (adapted with permission from [16]; copyright 2021 Korean Society for Fluid Machinery).

Response	R^2	RMSE
η	0.9898	2.7940×10^{-3}
$\sigma(T)$	0.9836	2.4497
T_{max}	0.8974	3.8560
$T_{average}$	0.9898	2.4947

2.5. Fan-Shaped Cooling Hole

The source term method used in this study is applicable to the cooling hole of the cylinder type, but not the fan-shaped hole. Hence, in order to investigate the effect of the fan-shaped hole on the cooling performance, it is necessary to make the full model, including the cooling system and perform numerical analysis. In this study, the cooling performance was compared by applying the 7-7-7 fan-shaped cooling hole of Schroeder and Thole [18] and the two holes designed by Seo et al. [19] to the result of the cooling hole arrangement design.

The 7-7-7 hole was named because the expansion angle in each direction was 7 degrees (the lateral half-angle was 7 degrees and the forward expansion was 7 degrees) [18]. Seo et al. [19] found the metering length, forward expansion angle, and lateral expansion angle to maximize the film cooling effectiveness based on this 7-7-7 hole. Design optimization was performed by numerical analysis and an experimental approach, separately, and the two fan-shaped hole geometries obtained in this way were called OPT(CFD) and OPT(EXP). They reported that because the expansion angle of these two holes was larger than that of the 7-7-7 holes, the coolant momentum at the cooling hole exit was reduced and the film cooling effectiveness was improved. Figure 9 shows these three types of fan-shaped holes applied to the nozzle vane, and more details can be found in reference [19].

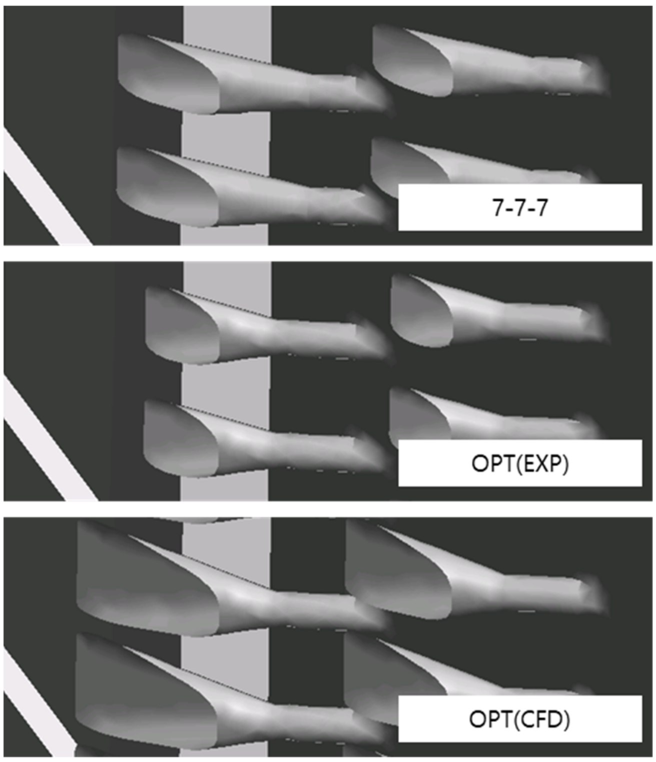

Figure 9. Three types of fan-shaped holes applied to the nozzle vane.

3. Results and Discussion

3.1. Results of the Cooling Hole Arrangement Design

The results of the cooling hole arrangement design derived through the process described in the previous chapter are summarized in Table 5. The row of "the full model" shows the numerical analysis results of the nozzle vane, including the cooling system, and that of "the approximate model" indicates the results obtained from the response surface model used in this design process. As shown in Table 5, the film cooling effectiveness (η), maximum temperature (T_{max}), and temperature uniformity (σ(T)) between the full model and the approximate model had slightly different values with similar tendencies. From this, it can be conjectured that approximate models used in the arrangement design adequately represent the design space, and the source term method also sufficiently produces the film cooling flow even if the cooling hole location is changed. Additionally, in the full model result, it can be confirmed that the design improved the film cooling effectiveness by 1.4%p, the average temperature by 0.9%, and the temperature uniformity by 4.0% compared with the base model.

Table 5. Results of the cooling hole arrangement design.

		Base Model	Design	Difference [%]
Full model	η	0.5342	0.5487	1.4457
	σ(T)	172.13	165.28	3.9795
	T_{max} [K]	1818.56	1824.96	0.3519
	$T_{average}$ [K]	1298.95	1286.04	0.9939
Approximate model	η	0.5559	0.5692	1.3305
	σ(T)	171.86	168.13	2.1748
	T_{max} [K]	1845.62	1840.93	0.2543
	$T_{average}$ [K]	1279.59	1267.71	0.9285

Figure 10 presents the film cooling effectiveness distribution of the base model and design. As the high temperature region on the leading edge and pressure side of the base model was significantly reduced, the film cooling effectiveness of the design was improved. This resulted from the shift in the cooling hole toward the leading edge, as shown in Table 6 and Figure 11. At the location of the cooling hole in Row6, the main flow splits into the pressure side and the suction side, so Row6 of the base model and the design remained at almost the same location. However, the adjacent rows of Row5 and 7 of the design were located closer to Row6 than to those of the base model. The difference in the temperature distribution between the base model and the design due to this cooling hole arrangement can be seen better in Figure 12. As the location of Row6 overlaps the stagnation points near the shroud, the discharged cooling fluid from Row6 directly faced the high temperature main flow, but because stagnation points near the hub were located between Row5 and 6, the high temperature region on the vane developed at that location. It can be confirmed that the high-temperature region at the leading edge near the hub was reduced in the design because the cooling hole of Row5 was located closer to Row6 than the base model. Furthermore, as all cooling holes on the pressure side after Row7 of the design moved in the upstream direction and the coverage of the cooling flow expanded, the design could have a lower average temperature than the base model. Eventually, this means that in order to decrease the temperature of the vane surface and improve the temperature uniformity, the region where the film cooling flow is difficult to reach should be reduced as much as possible.

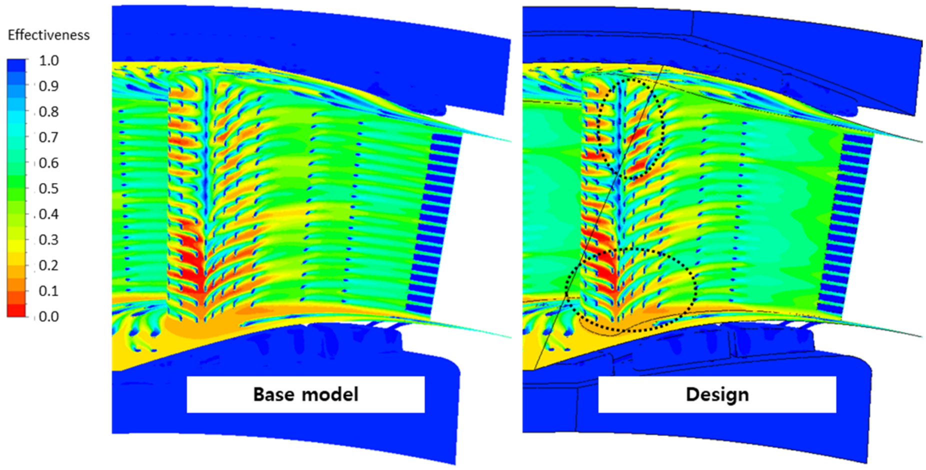

Figure 10. The film cooling effectiveness distribution for the base model and the design.

Table 6. Design results: design variables (normalized with the axial length of the airfoil; adapted with permission from [16]; copyright 2021 Korean Society for Fluid Machinery).

	Row1	Row2	Row3	Row4	Row5	Row6
Base model	0.3878	0.2893	0.1164	0.0288	0	0.018
Design	0.3395	0.2595	0.0795	0.021	0.001	0.017
	Row7	**Row8**	**Row9**	**Row10**	**Row11**	**Row12**
Base model	0.066	0.1273	0.1945	0.2917	0.5282	0.6951
Design	0.047	0.1047	0.1749	0.2571	0.4771	0.6771

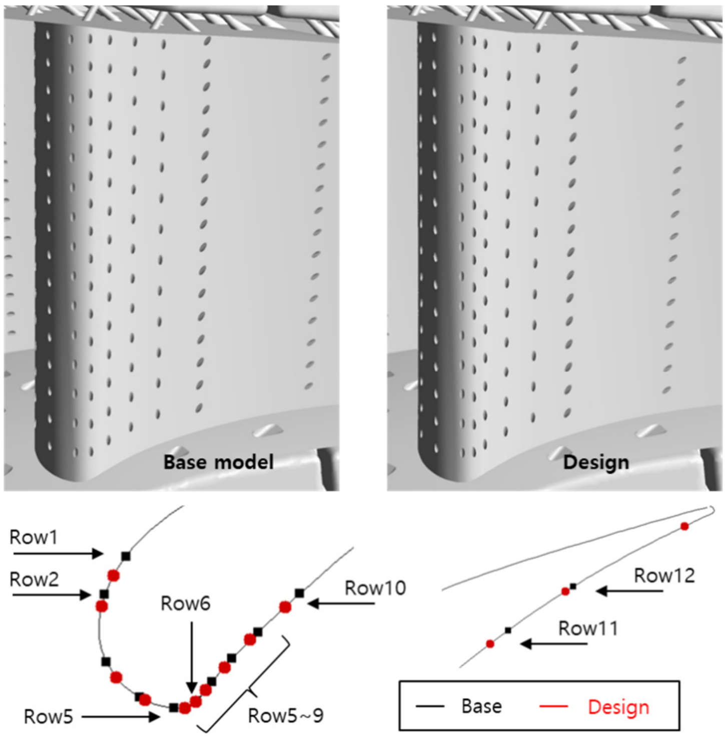

Figure 11. Comparison of cooling hole positions (adapted with permission from [16]; copyright 2021 Korean Society for Fluid Machinery).

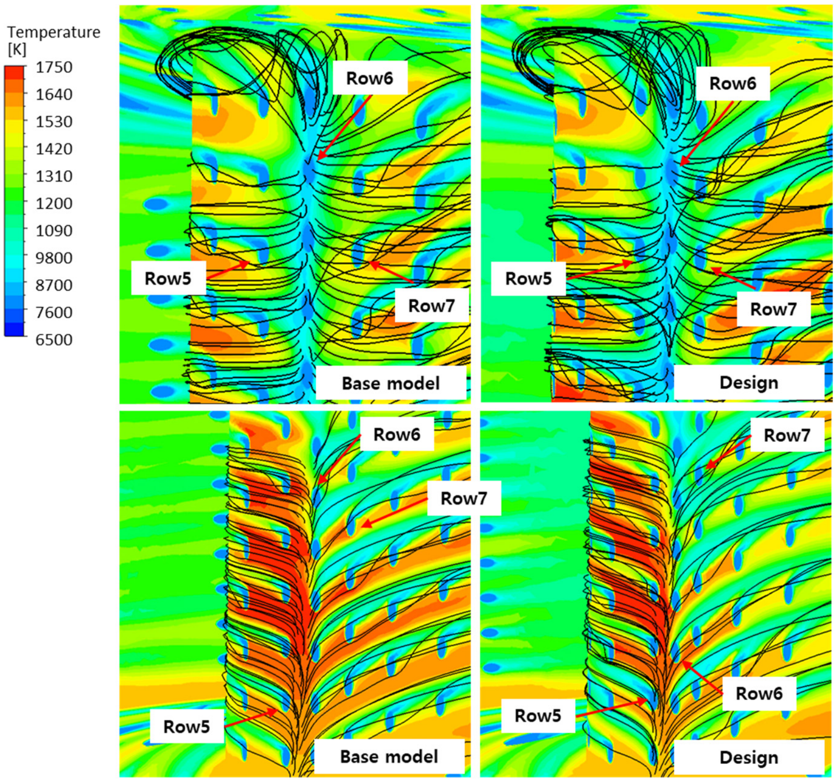

Figure 12. Temperature distribution and streamline around the leading edge (adapted with permission from [16]; copyright 2021 Korean Society for Fluid Machinery).

In order to verify the reliability of the aforementioned cooling flow rate model, the flow rates discharged from each cooling hole row of the design are compared in Figure 13. "Actual" is the value obtained through numerical analysis of the full model, including the cooling system, and "predicted" means the value of the cooling flow rate model that has been built with a neural network. The bar graph represents the sum of the cooling flow rates of each cooling hole in the same row. The line graph indicates the difference between the actual and predicted values, and is referred to in the vertical axis on the right. For every cooling hole row, the difference is within 6%, and especially Row6 and the adjacent rows show a high accuracy within a difference of 3%. Moreover, in the case of the cooling flow rate supplied from the forward cavity (connected to Row1~10) and the afterward cavity (Row11~13), as the difference was 2% and 0.4%, respectively, the predicted value of the cooling flow rate discharged from the vane was almost the same. From these, it was confirmed that the cooling flow rate model had the capability to predict the cooling flow rate with respect to the cooling hole location, and is reasonable for application to the cooling hole arrangement design.

3.2. Application of Fan-Shaped Holes

The fan-shaped type was applied only to the cooling holes from Row10 to Row12, which are available for space in the streamwise direction among the holes on the pressure side, as shown in Figure 14. The cylinder hole of Row10 to 12 was replaced with three types of fan-shaped holes at the same location as that of the design in Section 3.1, and the compound angle was removed. The film cooling effectiveness for three types is presented in Figure 15, and it shows a significant difference depending on whether or not the fan-shaped hole was applied. Especially, the film cooling effectiveness at the span 50% was improved by 0.3~0.4 when the fan-shaped hole was used, and the cooling hole named OPT(EXP) had the best cooling performance among them.

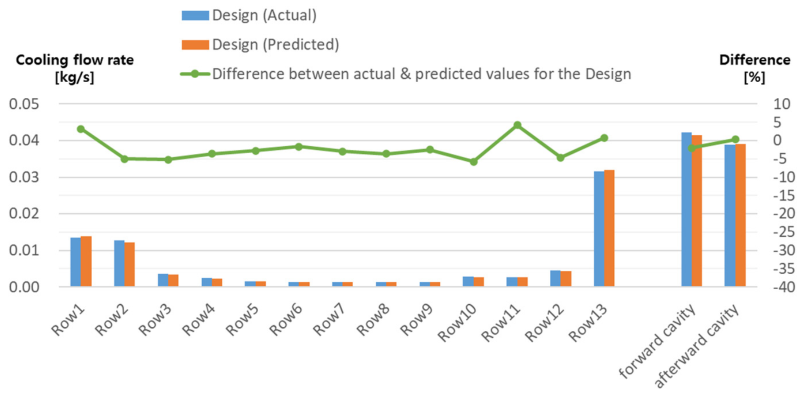

Figure 13. Cooling flow rate for the design (comparison between the actual and predicted values).

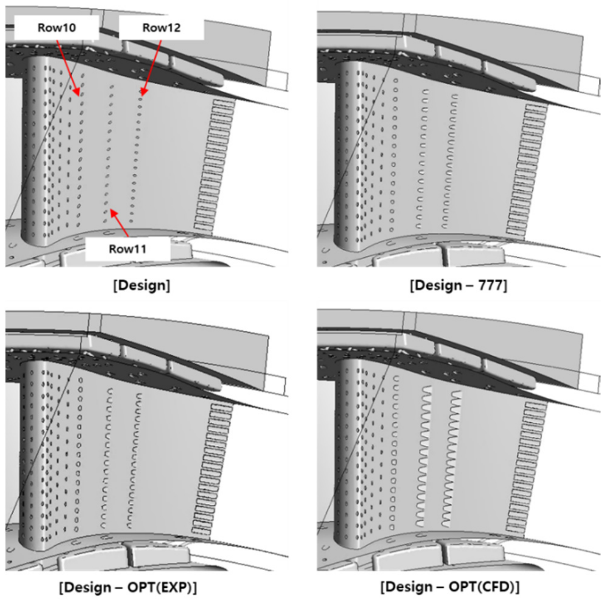

Figure 14. Temperature distribution and streamline around the leading edge.

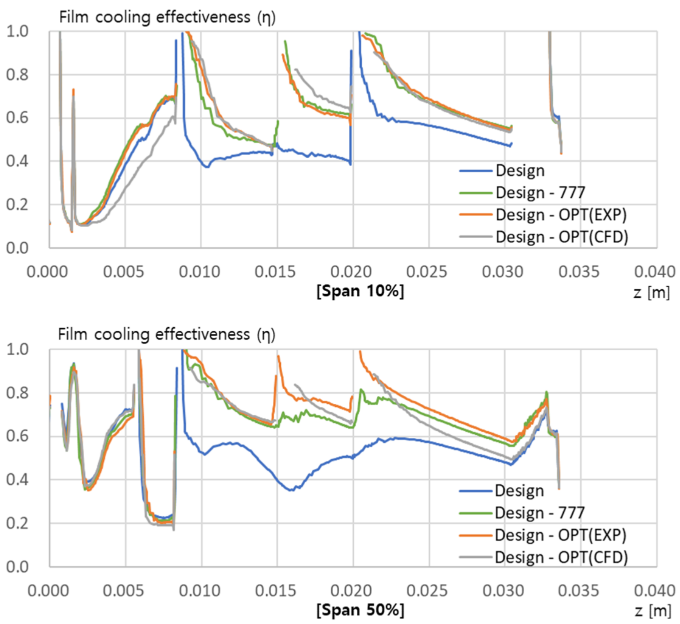

Figure 15. *Cont.*

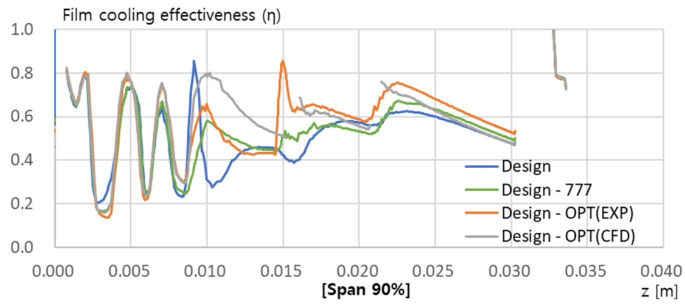

Figure 15. Film cooling effectiveness for the three types of the fan-shaped hole.

Figure 16 shows the behavior of the flow discharged from the fan-shaped hole. The film cooling effectiveness contour of the vane surface and the cross-sectional temperature distribution around the downstream of the fan-shaped hole are indicated. It can be seen that the cooling fluid ejected from the cylinder type cooling hole was farther away from the vane surface compared with that of the fan-shaped hole. This lift-off phenomenon of the cooling fluid was caused by the kidney vortex, and made the high temperature main flow permeate the space between the vane and the cooling fluid. As a result, the cooling performance of the film cooling was degraded. That is, compared with the cylinder hole, the film cooling effectiveness in the downstream of the fan-shaped hole was higher as the lift-off was suppressed. In addition, it can be confirmed that OPT(CFD) and OPT(EXP) holes with a large lateral expansion angle had a wider cooling coverage than the 7-7-7 hole.

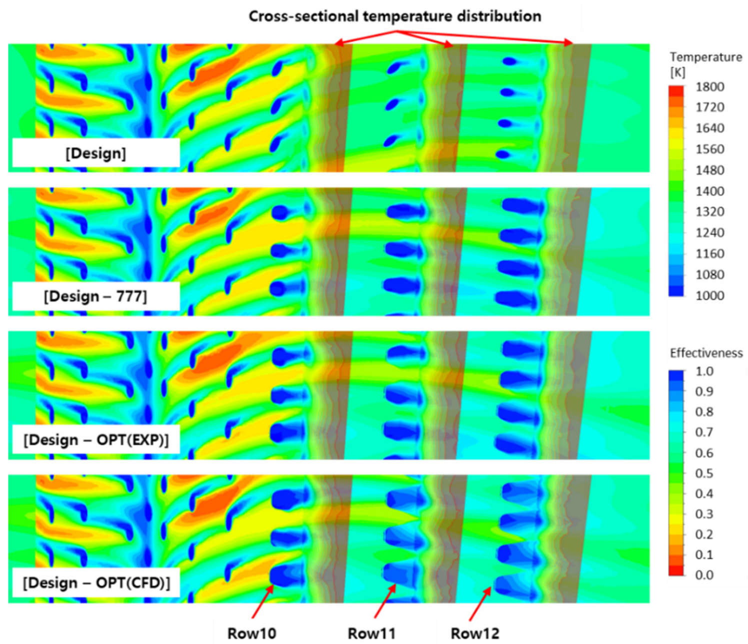

Figure 16. Cooling flow around the downstream of the cooling hole (film cooling effectiveness on the vane and cross-sectional temperature distribution).

The cooling flow rate at each cooling hole row of the base and final models is summarized in Table 7. The minus sign in "Difference" means that it decreased compared with the base model. Because the cooling hole location was changed, the cooling flow rate of the two models was different. For the cooling hole connected to the forward cavity, it is conjectured that the flow rate of Row10 increased as much as it decreased in Rows1 and 2. Therefore, the cooling flow rate in the forward cavity was almost the same for the base and final models. For the afterward cavity, the cooling flow rate decreased by 4%. From this variation, it can be inferred that the cooling performance was improved due to the application of the fan-shaped hole, not due to the increase in the cooling flow rate.

Table 7. The cooling flow rate at each cooling hole row of the base and final models.

	Base Model [kg/s]	Final Model [kg/s]	Difference [kg/s]	Difference [%]
Row1	1.3837×10^{-2}	1.3350×10^{-2}	-4.8624×10^{-4}	−3.51
Row2	1.3108×10^{-2}	1.2876×10^{-2}	-2.3190×10^{-4}	−1.77
Row3	3.8394×10^{-3}	3.7583×10^{-3}	-8.1084×10^{-5}	−2.11
Row4	2.4827×10^{-3}	2.5002×10^{-3}	1.7496×10^{-5}	0.70
Row5	1.4902×10^{-3}	1.5417×10^{-3}	5.1532×10^{-5}	3.46
Row6	1.3763×10^{-3}	1.2901×10^{-3}	-8.6212×10^{-5}	−6.26
Row7	1.2994×10^{-3}	1.3023×10^{-3}	2.9397×10^{-6}	0.23
Row8	1.3448×10^{-3}	1.3208×10^{-3}	-2.3930×10^{-5}	−1.78
Row9	1.3271×10^{-3}	1.3277×10^{-3}	6.3320×10^{-7}	0.05
Row10	2.7472×10^{-3}	3.3944×10^{-3}	6.4722×10^{-4}	23.56
Row11	2.8284×10^{-3}	2.8964×10^{-3}	6.7995×10^{-5}	2.40
Row12	4.6973×10^{-3}	4.6968×10^{-3}	-4.7400×10^{-7}	−0.01
Row13	3.1984×10^{-2}	3.0362×10^{-2}	-1.6228×10^{-3}	−5.07
Forward cavity	4.2851×10^{-2}	4.2662×10^{-2}	-1.8954×10^{-4}	−0.44
Afterward cavity	3.9510×10^{-2}	3.7955×10^{-2}	-1.5553×10^{-3}	−3.94

The results of these numerical analyses are quantitatively summarized in Table 8, and the film cooling effectiveness and the average temperature were computed with an area-average only for the pressure side, because those of the suction side did not change. The values in parentheses mean the difference from the design. The use of fan-shaped holes improves the film cooling effectiveness by approximately 4–7%p, but the temperature uniformity does not. This is because the temperature was locally decreased from the center of the pressure side to the trailing edge. However, considering that the uniformity of the base model was 172K, those of models that applied fan-shaped holes were still improved. For this reason, the final model of this study was selected as the nozzle vane model used the fan-shaped hole of OPT(EXP).

Table 8. Comparison of the cooling performance for the nozzle vane applied to the fan-shaped hole.

	Design	Design—777	Design—OPT(EXP)	Design—OPT(CFD)
η [1]	0.5082	0.5637 (5.5476%p)	0.5749 (6.6764%p)	0.5526 (4.4423%p)
$\sigma(T)$ [K]	165.28	170.05 (2.8860%)	170.84 (3.3640%)	169.82 (2.7469%)
T_{max} [K]	1824.96	1825.24 (0.0153%)	1820.18 (0.2619%)	1826.6 (0.0897%)
$T_{average}$ [K] [1]	1322.20	1272.66 (3.7468%)	1262.58 (4.5092%)	1282.53 (3.0003%)

[1] Area-averaged values on the pressure side.

3.3. Summary

The results of the base model, the design in Section 3.1 (Design), and the final model (Design-OPT(EXP)) are compared in Table 9. The values in parentheses show the difference from the base model. Compared with the base model, the final model had the film cooling effectiveness improved by 4.1%p and the average temperature decreased by 2.8%. Besides, compared with the design, that is, investigating the effect of applying the fan-shaped hole, the final model had the film cooling effectiveness improved by 2.7%p and the average temperature decreased by 1.8%. The maximum temperature of the Design almost did not change, and its uniformity improved by 4%. However, the uniformity of the final design was rather close to the base model. As mentioned above, this is because the temperature was locally reduced by replacing the cooling hole at only Row10 to 12 of the pressure side.

From these facts, it can be confirmed that compared with the cooling hole arrangement design, the application of the fan-shaped hole improved the film cooling effectiveness and average temperature, but the uniformity did not. If all cooling holes were replaced with a fan-shaped type, it can be expected that the uniformity would be improved. However, the uniformity degradation was unavoidable because the installation of this hole near the leading edge was difficult. Therefore, it is necessary to consider a compromise between the film cooling effectiveness (the average temperature) and the uniformity when applying a fan-shaped hole.

Table 9. Comparison of the cooling performance for the base model, the design in Section 3.1, and the final design.

	Base Model	**Design**	**Final Model Design—OPT(EXP)**
η	0.5342	0.5487 (1.4457%p)	0.5754 (4.1198%p)
σ(T) [K]	172.13	165.28 (3.9796%)	170.84 (0.7494%)
T_{max} [K]	1818.56	1824.96 (0.3519%)	1820.18 (0.0891%)
$T_{average}$ [K]	1298.95	1286.04 (0.9939%)	1262.16 (2.8323%)

4. Conclusions

In this study, the cooling design was performed to improve the cooling performance of the first stage nozzle vane of the E3 high-pressure turbine. The source term method and the cooling flow rate model were applied for the cooling hole arrangement design, and a numerical analysis was carried out on the full model, including the cooling system, to compare and verify the design results. Then, the effect of the fan-shaped hole application on the cooling performance was investigated. From the series of this process, the following conclusions could be drawn.

The final model with an improved cooling performance was derived. The film cooling effectiveness and the average temperature increased by 4%p and 2.8%, respectively. From the results of the cooling hole arrangement design, the high temperature region near the leading edge was significantly reduced as the cooling hole moved in the upstream direction, and the cooling performance on the pressure side was improved by changing the cooling hole of Rows10~12 to the fan-shaped type.

In the case of the temperature uniformity, it could be improved by 4% through the cooling hole arrangement design. However, after the fan-shaped hole was applied on the pressure side, the uniformity of the final model increased to that of the base model because the temperature was locally decreased. From this, it was found that the trade-off between the film cooling effectiveness (the average temperature) and the uniformity should be considered when a fan-shaped hole is applied.

Finally, the source term method and the cooling flow rate model introduced for this turbine nozzle cooling design were used to increase the efficiency and the degree of freedom for the design. In the cooling hole arrangement design, it could be confirmed that results from the approximate model had a similar trend with analysis results for the full model, and the predicted values from the cooling flow rate model had an error within 6%. Therefore, it is reasonable that these two methods were applied to the cooling design, and they are expected to be used more in research related to the film cooling hole flow.

Author Contributions: Conceptualization, S.J. and D.-H.R.; methodology, S.J., D.-H.R. and Y.S.K.; investigation, S.J. and H.C.; visualization, S.J.; writing—original draft preparation, S.J.; writing—review, D.-H.R., Y.S.K. and J.-H.K. All of the authors have read and agreed to the published version of the manuscript. All authors have read and agreed to the published version of the manuscript.

Funding: This research was supported by the National Research Foundation of Korea (NRF) funded by the Ministry of Science and ICT (no. NRF-2019K1A3A1A2009299).

Institutional Review Board Statement: Not applicable.

Informed Consent Statement: Not applicable.

Data Availability Statement: Not applicable.

Conflicts of Interest: The authors declare no conflict of interest.

References

1. Bunker, R.S. A Review of Shaped Hole Turbine Film-Cooling Technology. *J. Heat Transf.* **2005**, *127*, 441–453. [CrossRef]
2. Lee, S.; Rhee, D.H.; Cha, B.J.; Yee, K. Film Cooling Performance Improvement with Optimized Hole Arrangements on Pressure Side Surface of Nozzle Guide Vane—Part I: Optimization & Numerical Investigation. In Proceedings of the ASME Turbo Exposition, Seoul, Korea, 13–17 June 2016. ASME Paper No. GT2016-57975.
3. Jun, S.; Rhee, D.H.; Kang, Y.S. Application of Large Eddy Simulation to Turbine Nozzle with Film Cooling Holes. The KSFM. *J. Fluid Mach.* **2020**, *23*, 5–12.
4. Kang, Y.S.; Jun, S.; Rhee, D.H. Large Eddy Simulation on Film Cooling Flow from a Fan-Shaped Cooling Hole on a Flat Plate. The KSFM. *J. Fluid Mach.* **2018**, *21*, 1–9. [CrossRef]
5. Wang, Z.; Wang, Z.; Zhang, W.; Feng, Z. Numerical Study on Turbine Rotor Blade Unsteady Film Cooling Performance with Consideration of Inlet Non-Uniformities and Upstream Coolant. In Proceedings of the ASME Turbo Exposition, Phoenix, AZ, USA, 17–21 June 2019. ASME Paper No. GT2019-90723.
6. Johnson, J.J.; King, P.I.; Clark, J.P.; Ooten, M.K. Genetic Algorithm Optimization of a High-Pressure Turbine Vane Pressure Side Film Cooling Array. *J. Turbomach.* **2013**, *136*, 011011. [CrossRef]
7. Al-Zurfi, N.; Turan, A.; Nasser, A.; Alhusseny, A. A Numerical Study of Anti-Vortex Film-Cooling Holes Designs in a 1-1/2 Turbine Stage Using LES. *Propuls. Power Res.* **2019**, *8*, 275–299. [CrossRef]
8. Liu, J.; Du, W.; Hussain, S.; Xie, G.; Sundén, B. Endwall Film Cooling Holes Design Upstream of the Leading Edge of a Turbine Vane. *Numer. Heat Transf. Part A Appl.* **2021**, *79*, 222–245. [CrossRef]
9. Lee, S.; Yee, K.; Rhee, D.H. Optimum Arrangement of Film Cooling Holes Considering the Manufacturing Tolerance. *J. Propuls. Power* **2017**, *33*, 793–803. [CrossRef]
10. Zhang, Y.; Wang, K. A Study of Source Term Model for Full Coverage Film Cooling Simulation. In Proceedings of the ASME Turbo Exposition, Charlotte, NC, USA, 26–30 June 2017. ASME Paper No. GT2017-64607.
11. Gottiparthi, K.C.; Cao, C.; Sankaran, V. Modeling Effusion Cooling and Conjugate Heat Transfer Using Local Source Method. In Proceedings of the ASME Turbo Exposition, Charlotte, NC, USA, 26–30 June 2017. ASME Paper No. GT2017-91423.
12. Zhang, Z.; Chen, Z.; Su, X.; Yuan, X. Non-uniform Source Term Model for Film Cooling with the Internal Cross Flow. In Proceedings of the ASME Turbo Exposition, Virtual, 21–25 September 2020. ASME Paper No. GT2020-14404.
13. Yang, S.; Zhang, M.; Liu, Y.; Yang, J. Multi-objective Optimization of Turbine Blade Tip with Film Cooling Holes. In Proceedings of the ASME Turbo Exposition, Virtual, 7–11 June 2021. ASME Paper No. GT2021-60126.
14. Claus, R.W.; Beacg, T.; Turner, M.; Siddappaji, K.; Hendricks, E.S. *Geometry and Simulation Results for a Gas Turbine Representative of the Energy Efficient Engine (EEE)*; NASA/TM-2015-218408; NASA: Cleveland, OH, USA, 2015.
15. Timko, L.P. *Energy Efficient Engine High Pressure Turbine Component Test Performance Report*; NASA CR-168289; NASA: Cleveland, OH, USA, 1990.
16. Jun, S.; Rhee, D.H.; Kang, Y.S.; Chung, H.; Kim, J.H. Cooling Hole Arrangement Design of High Pressure Turbine for the Improvement of Cooling Performance. The KSFM. *J. Fluid Mach.* **2021**, *24*, 5–11.
17. *ANSYS CFX-Pre User's Guide 2020R1*; ANSYS Inc.: Canonsburg, PA, USA, 2020; pp. 207–216.
18. Schroeder, R.P.; Thole, K.A. Adiabatic Effectiveness Measurements for a Baseline Shaped Film Cooling Hole. In Proceedings of the ASME Turbo Exposition, Düsseldorf, Germany, 16–20 June 2014. ASME Paper No. GT2014-25992.
19. Seo, H.J.; Park, S.H.; Kwak, J.S.; Kang, Y.S. Experimental and Numerical Study on The Effect on Fan-Shaped Hole Configuration on Film Cooling Effectiveness. In Proceedings of the ASME Turbo Exposition, Phoenix, AZ, USA, 17–21 June 2019. ASME Paper No. GT2019-90817.